nature neuroscience

Goal-oriented searching mediated by ventral hippocampus early in trial-and-error learning

Sarah Ruediger[1,2], Dominique Spirig[1,2], Flavio Donato[1,2] & Pico Caroni[1]

Most behavioral learning in biology is trial and error, but how these learning processes are influenced by individual brain systems is poorly understood. Here we show that ventral-to-dorsal hippocampal subdivisions have specific and sequential functions in trial-and-error maze navigation, with ventral hippocampus (vH) mediating early task-specific goal-oriented searching. Although performance and strategy deployment progressed continuously at the population level, individual mice showed discrete learning phases, each characterized by particular search habits. Transitions in learning phases reflected feedforward inhibitory connectivity (FFI) growth occurring sequentially in ventral, then intermediate, then dorsal hippocampal subdivisions. FFI growth at vH occurred abruptly upon behavioral learning of goal-task relationships. vH lesions or the absence of vH FFI growth delayed early learning and disrupted performance consistency. Intermediate hippocampus lesions impaired intermediate place learning, whereas dorsal hippocampus lesions specifically disrupted late spatial learning. Trial-and-error navigational learning processes in naive mice thus involve a stereotype sequence of increasingly precise subtasks learned through distinct hippocampal subdivisions. Because of its unique connectivity, vH may relate specific goals to internal states in learning under healthy and pathological conditions.

Trial-and-error forms of learning and memory involve the deployment of complex individual learning sequences that lead to sustained modifications of behavior and efficient mastery of complex tasks[1,2]. Whether the learning sequences underlie principles reflected in the organization and recruitment of distinct brain systems has remained unclear. Trial-and-error learning has mainly been investigated in the context of striatal circuits, in which increasingly effective habits support optimization of learning processes, and it may be implemented by parallel loops of striatal subcircuits[3–7]. Accordingly, theoretical studies have predicted that complex trial-and-error tasks are best broken down into subtasks to be addressed independently by separate subsystems[8]. Further, studies of machine and animal learning have suggested that effective early search strategies should focus on local associations to goals, but whether and how such goal-oriented searching occurs has remained unclear[1,8].

The hippocampus provides an attractive system to investigate the notion that trial-and-error learning of biologically relevant tasks might involve the recruitment of functionally complementary subsystems. Thus, the hippocampus is of crucial importance in supporting trial-and-error navigation tasks that involve the rapid combination of episodes in space and time[9–11]. Furthermore, although local circuits are comparable throughout the hippocampus, the vH, intermediate hippocampus (iH) and dorsal hippocampus (dH) subdivisions differ substantially in tuning, connectivity, gene expression and function[12–19]. Gene-expression studies have revealed the existence of discrete spatial boundaries between principal neurons in vH, iH and dH, suggesting that the subdivisions reflect discrete entities[14,15,17]. On the basis of their connectivity in distinct brain networks[15,20,21], vH (anterior in humans) is thought to be more concerned with emotions and body states[15], whereas dH (posterior in humans) has predominantly visuo-spatial and cognitive functions[12–16]. Although dH is important in spatial learning[12,13,16], the function of vH in learning has remained less clear[15]. This might be because most studies have focused on the endpoints of complex hippocampus-dependent tasks, which are often highly spatial and cognitive, and on average population performances instead of how individual animals learn a task.

Hippocampal learning can be associated with a robust local growth of new excitatory synapses by large mossy fiber terminals (LMTs) in CA3 onto fast-spiking GABAergic interneurons (FFI growth), which are crucial for memory precision[22]. The new synapses do not stabilize in mice lacking β-adducin[23], and local virus-mediated reintroduction of β-adducin in granule cells restores structural plasticity and memory precision[22]. At the physiological level, FFI growth is required to recruit comparatively small ensembles of pyramidal neurons expressing the transcription factor c-Fos in CA3 upon learning, a function that seems to underlie the role of FFI growth in memory precision[22]. Here we exploited these structural traces of learning to map and probe the involvement of hippocampal subdivisions during navigational learning. We investigated longitudinally how individual naive laboratory mice learn to navigate a Morris water maze[24] and combined these detailed behavioral analyses with anatomical and local genetic-rescue studies to dissect the roles of the hippocampal subdivisions in this complex trial-and-error learning process.

RESULTS

Individual mouse strategies reveal three learning phases

We first analyzed the average learning patterns of mice in the Morris water maze. In this task a platform is hidden at a fixed position in the water, and mice are released facing the wall at different positions in the circular maze. Performance is recorded as time to locate the

[1]Friedrich Miescher Institute, Basel, Switzerland. [2]These authors contributed equally to this work. Correspondence should be addressed to P.C. (caroni@fmi.ch).

Received 30 July; accepted 21 August; published online 23 September 2012; doi:10.1038/nn.3224

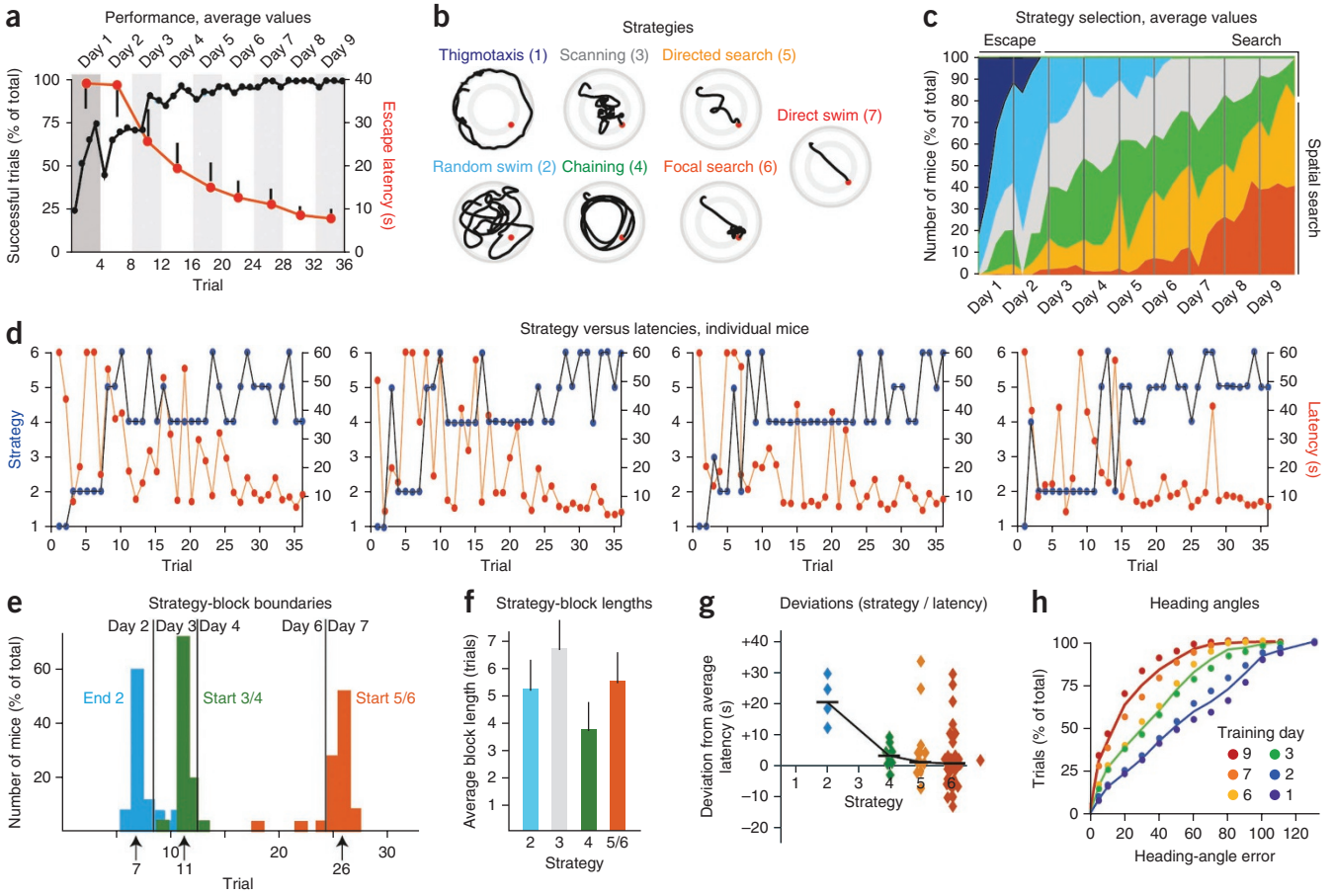

Figure 1 Sequential deployment of search-strategy habits during water maze learning. (**a**–**c**) Behavioral analysis of water maze learning at the population level. Mean values for 30 mice. Performance (**a**) was evaluated as average escape latency and percentage of successful trials at each trial and training day. A schematic representation and color code for each strategy (**b**) and the average prevalence of each strategy by trial number (**c**) are shown. (**d**–**h**) Behavioral analysis of water maze learning in individual mice. (**d**) Strategy and latency versus trial number for four representative mice. (**e**) Distribution of strategy-block boundaries for 25 individual mice, with percentages of mice for which block 2 (blue) ended and blocks 3 or 4 (green) and 5 or 6 (orange) began, represented as a function of trial number. (**f**) Total block-length values for individual mice, averaged over 25 mice. (**g**) Extent to which the latencies of individual trials involving the exploration of alternative strategies differed from the mean latencies for that phase of the training process. The individual values represent the latency deviations for individual trials, ordered according to the strategy of the exploratory trials (25 mice; see Online Methods). (**h**) Prevalence of heading-angle error by training day. Cumulative plots; four trials per day, 25 mice. Each dot represents the relative incidence of angles ranging between two consecutive data points (for example, between 20° and 10°). The colored lines highlight learning phases and connect averages for indicated training day intervals. Error bars, s.e.m.

platform (escape latency) during training trials (**Fig. 1a**), and spatial memory is assayed as persistence in searching the platform quadrant in the absence of the platform (reference memory)[12,24]. In addition to these conventional readouts, and to augment the power of the analysis, we categorized the behavior of individual mice according to the incidence of distinct search strategies[25–27] as a function of training trial (**Fig. 1b** and Online Methods). Consistent with previous reports[24–26], this detailed behavioral analysis revealed that mice applied qualitatively different search strategies as they became more proficient at this spatial task: global (random swim) and then local search strategies (scanning and chaining) were predominant during early phases of learning, and spatial search strategies (directed search, focal search and direct swim) took over during late phases (**Fig. 1c**). Average latencies and strategies evolved continuously as a function of trial number (**Fig. 1a,c**).

We then analyzed the learning curves of individual mice. In contrast to what could be detected at the population level, individual mice showed notable search habits, consisting of repeated use of the same search strategy in at least three consecutive trials (see Online Methods), interrupted by one or two trials involving alternative, and in most cases more 'advanced,' strategies (**Fig. 1d**). Individual latency curves oscillated substantially during the first half of the learning process (**Fig. 1d**). To provide average measures of these individual behaviors, we then determined whether features of the search habits were shared among cohorts of mice during learning. A detailed analysis of 28 individual learning curves revealed that the majority of mice (21/28) ended a first block, involving strategy 2 (random swim) after trial 7 (just before the end of day 2), and initiated a second block, involving strategy 3 (scanning) or 4 (chaining) at trial 10–12 (during day 3), which was followed by a third series of blocks involving strategies 5 and 6 (directed search and focal search, respectively; denoted as 5/6) during trials 22–26 (between days 5 and 7) (**Fig. 1e**). The majority of mice (25/28) showed a strategy progression of 2-4-5/6 (13/25) or 2-3-5/6 (8/25), and a smaller fraction of mice (3/28) showed a 2-5/6 pattern (**Fig. 1d**, right, and **Supplementary Fig. 1**). Among different cohorts of mice, individual search habits seemed to begin and end at comparable stages during learning. Consistent with this notion, average total block lengths per mouse for each search habit were also comparable (strategy 2: 5.2 ± 1.2 trials; strategy 3: 6.7 ± 0.95 trials; strategy 4: 3.65 ± 0.85 trials; strategies 5/6: 5.46 ± 1.17 trials (s.e.m.);

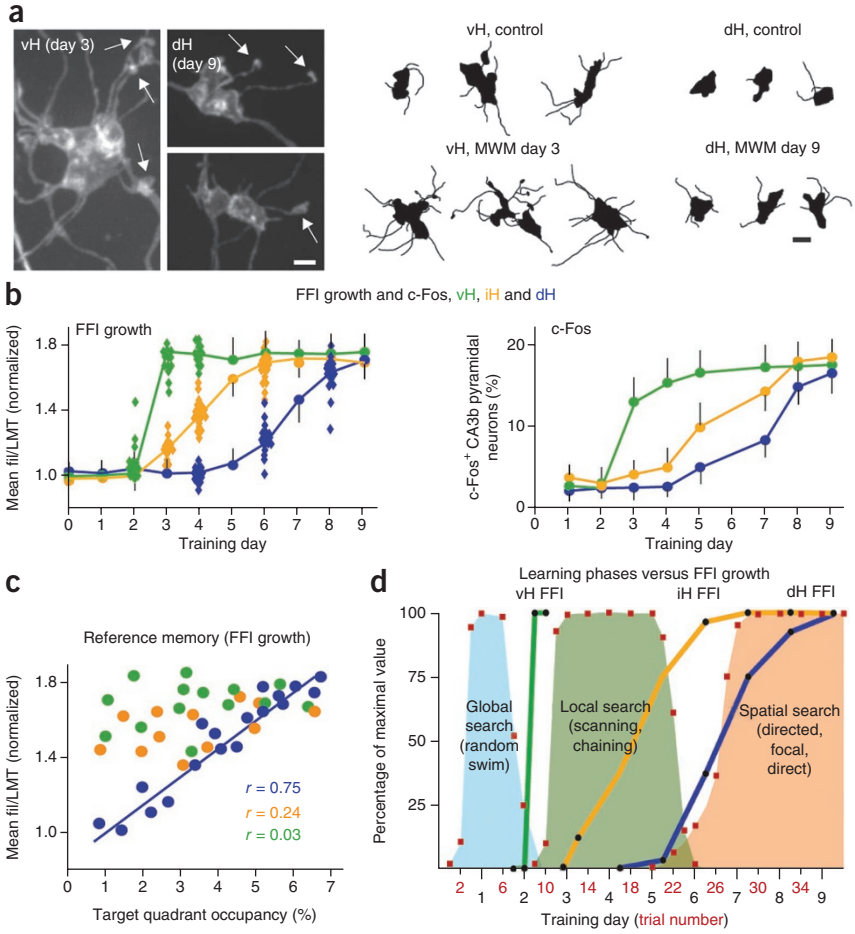

Figure 2 Sequential recruitment of hippocampal subdivisions during maze learning. (**a**) Representative examples of GFP-positive LMTs (left, photographs; right, camera lucida drawings) in CA3b of vH and dH on days 3 and 9, respectively, of the maze training procedure (MWM). Arrows indicate varicosities (putative presynaptic terminals[22]) at the tips of filopodia. Scale bars, 5 µm. (**b**) FFI growth (left) and percentage of c-Fos$^+$ CA3b pyramidal neurons (right) in vH, iH and dH during maze training. n = 6–10 mice. Individual dots at days 2, 3, 4, 6 and 8: filopodia/LMT values for individual mice shown for transition time points (left). (**c**) FFI growth at dH (but not iH or vH) is correlated to spatial learning (reference memory). Fil, filopodia. Target quadrant occupancy, percentage of test time spent in target quadrant (values are given as 1/10 of actual percentage). Dots represent values for individual mice, collected between day 5 and day 9 of the training procedure. (**d**) Schematic illustration of the relationship between the prevalence of search-strategy habits (blue, green and orange areas) and FFI growth at vH, iH and dH as a function of trial number (for search habits; red) and training day (for FFI growth; black) during maze learning. Individual values are averages from the data shown in **b** and **Figure 1e**. Error bars, s.e.m.

Fig. 1f and Online Methods). Furthermore, even when mice explored alternative strategies during a particular search habit, corresponding individual latencies matched average values for the particular learning phase across the mouse cohort (**Fig. 1g**). Finally, a population analysis of initial heading-angle errors as a function of training day (see Online Methods) provided additional independent evidence that progress during the maze learning process had some discontinuous features, with prominent improvements again occurring between days 2 and 3 and between days 6 and 7 (**Fig. 1h**). Taken together, these results suggested that the learning processes of individual naive mice might involve learning phases characterized by distinct search habits. In most mice, the learning phases corresponded to training days 1–2 (trials 1–8; first phase: blocks of strategy 2, >50% of trials with heading-angle errors >50°), days 3–6 (trials 9–24; second phase: blocks of strategies 3 and 4, >50% of trials with heading-angle errors <30°) and days 7–9 (trials 25–36; third phase: blocks of strategies 5/6, >50% of trials with heading-angle errors <10°).

FFI growth at hippocampal subdivisions during learning

To investigate the neural basis of the sequential phases of maze learning, we investigated hippocampal patterns of FFI growth at LMTs in CA3b (ref. 22). Cohorts of mice underwent repeated daily training periods of different total durations (four trials per day, as described above), and we determined values for number of filopodia per LMT (filopodia/LMT) on the day after the final training day. We detected distinct baselines and learning-related patterns of filopodia/LMT values in vH, iH and dH (mean baseline number of filopodia/LMT = 1.74 ± 0.1 (dH), 2.32 ± 0.1 (iH) and 3.11 ± 0.15 (vH); **Fig. 2a**,**b** and **Supplementary Fig. 2**; see Online Methods). In vH, filopodia/LMT values increased abruptly after day 2 (in 12/12 mice analyzed) and reached plateau levels 1.8-fold higher than ventral baseline values by day 3 (**Fig. 2b**). No filopodial increases were detected at 1 h or 4 h after the last trial on day 2, suggesting that this FFI growth reflected an overnight memory consolidation process (data not shown). The marked increase in synapse numbers was accompanied by a corresponding increase of c-Fos recruitment upon training in CA3b pyramidal neurons from day 3 in vH (percentage of c-Fos$^+$ vH neurons = 2.34 ± 1.2 (day 1) and 3.2 ± 1.6 (day 2), not significant (n.s.), and 13.4 ± 2.4 (day 3), $P < 0.001$; **Fig. 2b**). In iH, filopodial growth was first detectable on day 3 and increased gradually to reach plateau values (also ~1.8-fold higher than intermediate baseline levels) by day 5–6 (**Fig. 2b**). FFI growth in iH was specifically correlated to increasing c-Fos recruitment upon training in the same subdivision (percentage of c-Fos$^+$ iH neurons = 2.68 ± 1.3 (day 3) and 16.95 ± 1.7 (day 6), $P < 0.01$; **Fig. 2b**). Finally, in dH, filopodia/LMT values did not increase significantly up to day 5 of the training protocol, and then they increased gradually to reach plateau values (also ~1.8-fold higher than dorsal baseline values) at day 8–9 (percentage of c-Fos$^+$ dH neurons = 1.8 ± 1.2 (day 1) and 15.4 ± 2.2 (day 9), $P < 0.01$; **Fig. 2b**). As with vH and iH, FFI growth in dH was specifically correlated to increased c-Fos recruitment in that hippocampal subdivision (percentage of c-Fos$^+$ dH neurons = 1.8 ± 1.2 (day 1) and 15.4 ± 2.2 (day 9), $P < 0.01$; **Fig. 2b**). Furthermore, FFI growth in dH was correlated with the quality of reference memory in individual mice, whereas FFI growth in vH and iH was not (Pearson correlation r = 0.75 (dH), $P < 0.001$ and 0.24 (iH) and 0.03 (vH), n.s.; **Fig. 2c**).

We compared how average search-strategy habit distributions (per trial number) and FFI growth at hippocampal subdivisions (per day) evolved during maze learning (**Fig. 2d**). In most mice, vH FFI growth (beginning at day 3) anticipated the onset of local search habits such as scanning and chaining (at trial 10, >80% of mice) (**Fig. 2d**). Gradual FFI growth at iH (from day 3 to day 6) coincided with the deployment

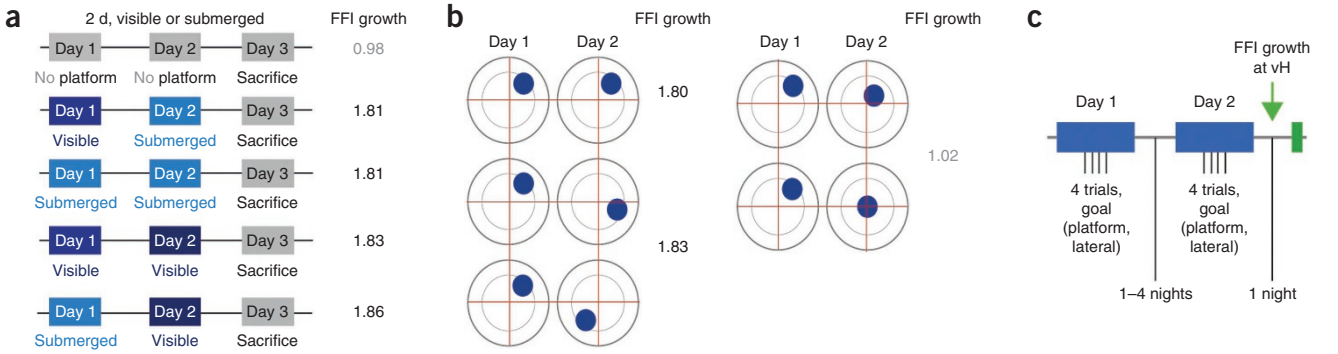

Figure 3 Specific task-goal association reflected by vH FFI growth during maze learning. (**a**) Analysis of experimental conditions (platform submerged, visible or absent) that produce FFI growth (fold increase) at vH. (**b**) Influence of platform position constancy on vH FFI growth. Moving a visible platform to a new position at a comparable distance from the wall on day 2 did not compromise FFI growth on day 3 (left), whereas moving the platform toward the center of the maze on day 2 suppressed FFI growth on day 3 (right). Mean values; $n = 5–8$ mice. (**c**) Schematic of requirements for FFI growth at vH.

of local search habits and reached plateau values when most mice had switched to spatial search habits. Finally, gradual FFI growth in dH coincided with the consistent deployment of spatial search strategies. Together, these findings suggested that, in mice, trial-and-error learning to navigate a water maze involves a stereotyped sequence of learning phases. These results were consistent with a specific role for dH in fine-scale spatial-map learning late in maze navigation and suggested that vH and iH may have distinct and sequential roles during earlier phases of maze learning.

vH FFI growth and the learning of specific task-goal associations

We next sought to determine what aspects of trial-and-error tasks might be learned through vH. Because this hippocampal subdivision is connected to goal-related networks, and recent studies have provided evidence that it contains single units tuned to goal[15,18,19], we explored the possibility that vH might support the learning and implementation of specific associations between invariant features of the task and reward-related goal[28]. To this end, we first investigated mice that underwent a novel-object recognition task in the absence or presence of a positive food reward. In the absence of reward (incidental learning), mice did not show alterations in novel-object discrimination in subsequent training sessions or alterations in filopodia/LMT values in vH or dH (**Supplementary Fig. 3**). By contrast, when a food reward was repeatedly associated with the familiar object, relative exploration time for the familiar object increased gradually beginning on day 3–4 (**Supplementary Fig. 3**). Furthermore, beginning on day 11–12, but not yet on day 10, mice showed a strong preference for the familiar object, even in the absence of food reward (reference memory). Notably, mean filopodia/LMT values increased selectively between days 10 and 12 in vH but not dH, and the vH increase was closely correlated with reward-controlled learning in individual mice (**Supplementary Fig. 3**; see Online Methods). These results provided evidence that conversion of an incidental goal-free task into a reward-based one is sufficient to induce FFI growth at vH upon behavioral learning (tested as reference memory). Because acquisition of a behavioral bias and FFI growth were closely correlated at the individual level in mice, the results further suggested that FFI growth occurred in vH within 1 d of bias learning in these experiments.

In further experiments aimed at determining whether FFI growth in vH depends on behavioral learning of hippocampal associations to reinforcers, we carried out fear-conditioning experiments (negative reward) under normal light conditions (contextual conditioning, hippocampus dependent) and in complete darkness (conditioning to explicit cues, not hippocampus dependent). We found that, whereas mice that underwent contextual fear-conditioning showed FFI growth in vH and dH, those that had been conditioned in the dark froze when re-exposed to the same odor or cage floor but did not show alterations in mean filopodia/LMT values or c-Fos recruitment in vH or dH (**Supplementary Fig. 3**; see Online Methods). These results were reminiscent of the perceptual requirements for hippocampal encoding[29] and suggested that FFI growth upon behavioral learning is induced in vH only if the behavioral protocol involves conditions producing hippocampal associations between context and reward.

We then determined whether vH FFI growth during maze navigation might involve learning about a specific task-goal relationship[28]. As we expected, when we subjected mice to the maze protocol in the absence of a platform (and, hence, in the absence of a reward-related goal), we did not observe an increase in vH filopodia/LMT values at any time (filopodia/LMT = 3.25 ± 0.2 (naive mice) and 3.29 ± 0.3 (after 2 d of free swim), n.s.; **Fig. 3a**). We further found that (i) omitting the platform on the first or second day of training suppressed FFI growth; (ii) 2 d of training, each involving four trials, were required for FFI growth; (iii) the second day of training did not have to immediately follow the first day to elicit FFI growth and (iv) introduction of a goal-free training day between the first and second day of goal-oriented learning inhibited ventral FFI growth after the second platform training day (**Supplementary Fig. 4**). Further supporting an association between vH FFI growth and reward-related goals, the extent of induction of vH FFI growth was indistinguishable whether the platform was hidden or visible (**Fig. 3a**). Notably, however, when the position of a visible platform was changed from a peripheral position on day 1 to positions closer to the center of the pool on day 2, no vH FFI growth was detected on day 3, suggesting that the structural plasticity might reflect learning about a specific association between the platform and its distance from the wall (**Fig. 3b**, right). In support of this interpretation, changing the position of the visible platform with respect to the external cues while keeping it within a comparable distance from the pool wall did not suppress vH FFI growth on day 3 (**Fig. 3b**, left). Taken together, these results suggested that, in maze learning, structural plasticity in vH on day 3 might involve establishing a consistent association on day 1 between the goal (the platform) and a specific aspect of the task (for example, the distance of the platform from the wall) and confirming that association on day 2 (**Fig. 3c**).

To provide additional evidence that FFI growth at vH involves a classical reward mechanism, we interfered with signaling by the reward neuromodulator dopamine[30] and its D1/D5 receptor during water maze learning[31]. To this end, the D1/D5 antagonist SCH23390 was

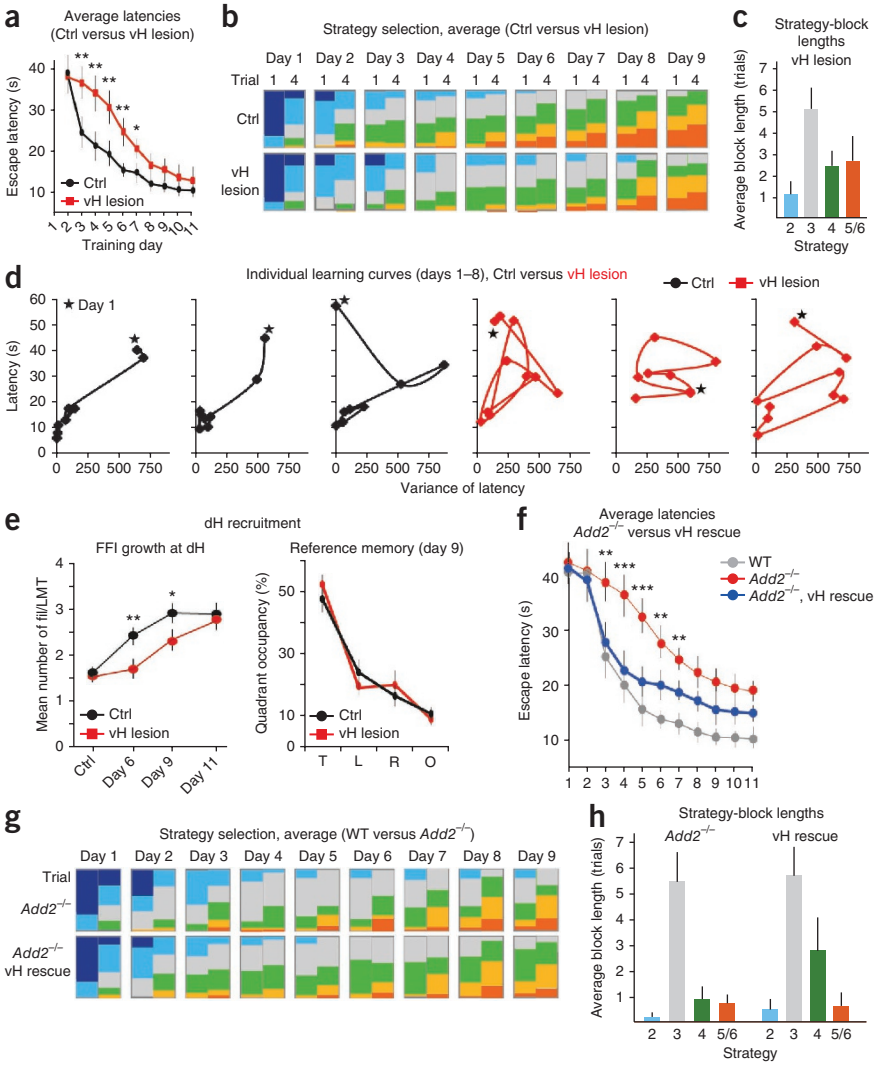

Figure 4 Role of vH in water maze learning. (**a**,**b**) Population-level analysis of latencies (**a**) and strategies (**b**) in mice with excitotoxic lesions of vH (vH lesion) versus controls. To highlight progress within and between days, the strategy plot (**b**) reflects the mean strategy-recruitment values for the first and fourth trials of each day. Analysis in **a**,**b** as described in **Figure 1c**; $n = 15$ mice. (**c**) Strategy-block lengths for mice with vH lesions, as described in **Figure 1f**. (**d**) Enhanced variability of individual trials during maze learning in mice with vH lesion versus controls. Latency versus latency variance is plotted for three individual mice each. Stars indicate values for training day 1; lines connect values from day 1 to day 8. (**e**) Delayed but undiminished dH FFI growth and reference memory in vH-lesioned mice. T, target; L, left; R, right; O, opposite. $n = 4$ (FFI growth) and 15 (reference memory). (**f**–**h**) Learning with FFI growth restricted to vH. Impaired maze learning in *Add2*$^{-/-}$ mice and specific rescue of early learning phase upon reintroduction of β-adducin into granule cells of vH. Population- and individual-level analysis was done as described in **a**–**c**. $n = 12$ mice. WT, wild type; Ctrl, controls injected with vehicle only; fil, filopodia. Error bars, s.e.m.; $^{*}P < 0.05$, $^{**}P < 0.01$, $^{***}P < 0.001$.

applied systemically 20 min before each training day, and control mice were treated with vehicle lacking the drug. The antagonist interfered with learning and strategy selection throughout the training procedure and completely blocked FFI growth in vH (**Supplementary Fig. 4**).

Function of vH in water maze learning

Having defined task features that lead to FFI growth at vH early during maze training, we next addressed the function of this hippocampal subdivision during water maze learning. We reasoned that all hippocampal subdivisions might synergistically contribute to the learning process throughout training or that each subdivision might make its main, specific contribution at a distinct phase of the learning process.

We first analyzed mice with excitotoxic bilateral lesions of vH. All mice included in the analysis had nearly complete lesions of vH CA3 (and CA1) and <15% losses at iH CA3 (**Supplementary Fig. 5**). Ventrally lesioned mice showed strongly compromised latency values at days 3–5 of training (day 3 escape latency = 23.2 ± 5.5 s (vehicle) versus 36.5 ± 4.1 s (vH lesion), $P < 0.01$) and improved later to reach values comparable to controls at days 10–11 (day 10 escape latency = 10.3 ± 2.2 s (vehicle) versus 12.2 ± 3.1 s (vH lesion), n.s.; **Fig. 4a**). Ventrally lesioned mice also showed disruption of the progression of local search-strategy deployment during days 2–4 (use of strategy 4 on day 4 = 28 ± 3.3% of trials (vehicle) versus 15 ± 6.5% (vH lesion), $P < 0.01$), and a delayed onset of spatial search strategies, but use of those strategies during late phases of maze learning was comparable to that of control mice (use of strategy 5 and 6 on day 9 = 33 ± 3.8% of trials (vehicle) versus 29 ± 5.1% (vH lesion), n.s.; **Fig. 4b**). Strategy habits were less prominent in vH-lesioned mice; random swim was particularly affected by the lesions, whereas scanning habits were comparatively preserved (**Supplementary Fig. 1** and **Fig. 4c**). Furthermore, vH lesions led to a loss of correlation between single-trial strategies, single-trial latencies and mean latencies (**Supplementary Fig. 6**). In what is probably reflective of this inconsistency in trial latencies, individual lesioned mice had notably unpredictable trajectories of daily variation in latency through most of the training procedure (**Fig. 4d**). In spite of these disruptions in performance consistency, ventrally lesioned mice showed delayed but ultimately normal reference memory[16] and extents of FFI growth in dH (**Fig. 4e**). These results suggest that vH is important in learning during days 2–5, when global and local search strategies predominate, and in search and performance consistency throughout maze learning.

To further define the function of vH in maze learning, we devised experiments in which learning-related FFI growth was confined to vH. In mice lacking the actin cytoskeleton–cell cortex linker protein β-adducin (*Add2*$^{-/-}$), which are deficient in learning-related FFI growth and synaptogenesis[23,32], improvements in latency were reduced throughout the maze learning procedure (day 3 latency = 24.5 ± 1 s (wild type) versus 38.3 ± 3.4 s (*Add2*$^{-/-}$), $P < 0.01$; day 5 latency = 14.8 ± 3.2 s (wild type) versus 32.1 ± 2.6 s (*Add2*$^{-/-}$), $P < 0.001$; day 7 latency = 12.3 ± 2 s (wild type) versus 23.8 ± 2.3 s (*Add2*$^{-/-}$), $P < 0.001$; **Fig. 4f**,**g**). Furthermore, *Add2*$^{-/-}$ mice showed very few learning-related habits throughout training (**Fig. 4h**). In *Add2*$^{-/-}$ mice in which β-adducin had been reintroduced locally in vH (but not iH or dH) granule cells

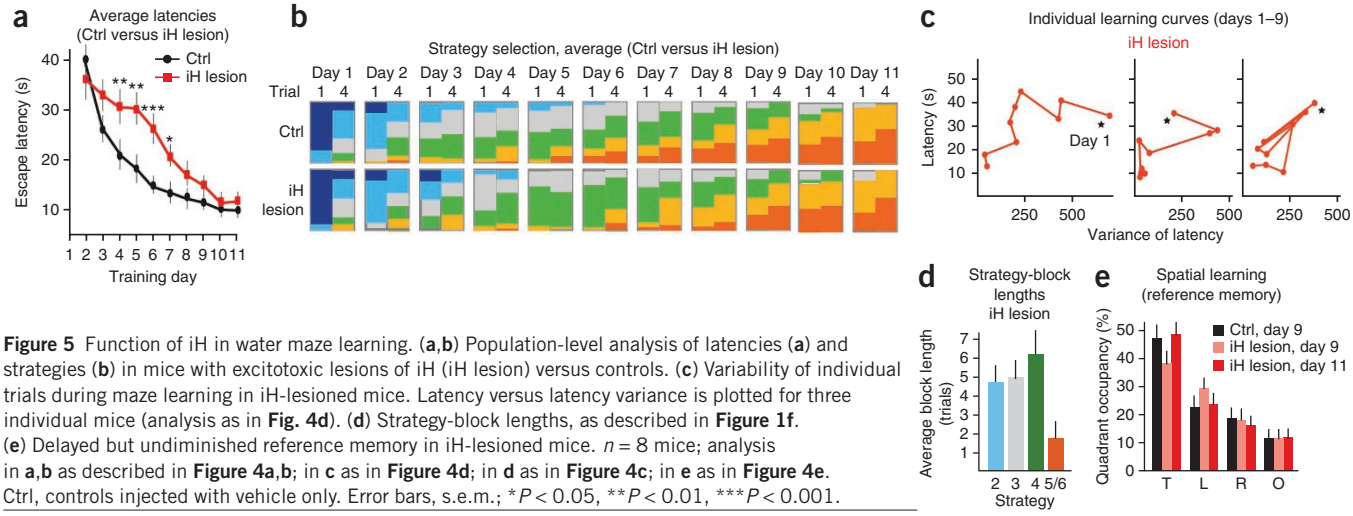

Figure 5 Function of iH in water maze learning. (**a**,**b**) Population-level analysis of latencies (**a**) and strategies (**b**) in mice with excitotoxic lesions of iH (iH lesion) versus controls. (**c**) Variability of individual trials during maze learning in iH-lesioned mice. Latency versus latency variance is plotted for three individual mice (analysis as in **Fig. 4d**). (**d**) Strategy-block lengths, as described in **Figure 1f**. (**e**) Delayed but undiminished reference memory in iH-lesioned mice. $n = 8$ mice; analysis in **a**,**b** as described in **Figure 4a**,**b**; in **c** as in **Figure 4d**; in **d** as in **Figure 4c**; in **e** as in **Figure 4e**. Ctrl, controls injected with vehicle only. Error bars, s.e.m.; $^{*}P < 0.05$, $^{**}P < 0.01$, $^{***}P < 0.001$.

using a lentivirus expressing a β-adducin–green fluorescent fusion protein (GFP–β-adducin)[23], learning-related FFI growth was specifically rescued in vH (day 3 filopodia/LMT = 2.78 ± 0.3 (*Add2*$^{-/-}$) versus 5.96 ± 0.3 (vH rescue), $P < 0.0001$; **Supplementary Fig. 7**). Supporting the notion that behavioral learning involving vH is crucial specifically during early phases of maze learning, ventral rescue restored average latency and strategy curves to wild-type values beginning on day 3 and continuing until day 5 of training (day 5 latency = 14.8 ± 3.2 s (wild type) versus 20.1 ± 4 s (vH rescue), n.s.), whereas further improvements beyond that early phase were still inhibited (day 11 latency = 10.2 ± 1.1 s (wild type), 19.4 ± 1.9 s (*Add2*$^{-/-}$) and 16.1 ± 1.7 (vH rescue), $P < 0.05$; **Fig. 4f**,**g**). The analysis of individual mice revealed that the second learning phase (local search habits) was specifically rescued (average block length for strategy 4 = 3.65 ± 0.85 (wild type) and 1.1 ± 0.41 (*Add2*$^{-/-}$), $P < 0.01$, and 2.45 ± 1.1 (vH rescue), n.s.), whereas the first phase (average block length for strategy 2 = 5.2 ± 1.2 (wild type); 0.2 ± 0.1 (*Add2*$^{-/-}$), $P < 0.001$, and 0.51 ± 0.4 (vH rescue), $P < 0.01$) and the third phase (average block length for strategies 5/6 = 5.46 ± 1.2 (wild type), 0.84 ± 0.3 (*Add2*$^{-/-}$), $P < 0.001$, and 0.76 ± 0.4 (vH rescue), $P < 0.001$)) were not (**Supplementary Fig. 1** and **Fig. 4h**).

Function of iH in water maze learning

To investigate the function of iH in maze learning, we analyzed mice with complete bilateral excitotoxic lesions of iH (**Supplementary Fig. 5**). None of the mice showed neuronal losses extending >10% into the anterior-posterior extension of adjacent vH or dH (**Supplementary Fig. 5**). The learning curves of mice with iH lesions were specifically delayed between day 4 and day 7 of the learning process, and iH-lesioned mice reached latency values comparable to non-lesioned controls by day 11 (day 11 latency = 9.8 ± 2 s (vehicle) and 11.4 ± 2 (iH lesion), n.s.; **Fig. 5a**,**b**). iH-lesioned mice showed much smaller variations in latency across individual trials than vH-lesioned mice (**Fig. 5c**; compare to **Fig. 4d**). A strategy analysis revealed a very prolonged deployment of local search habits (scanning and chaining; average block length for

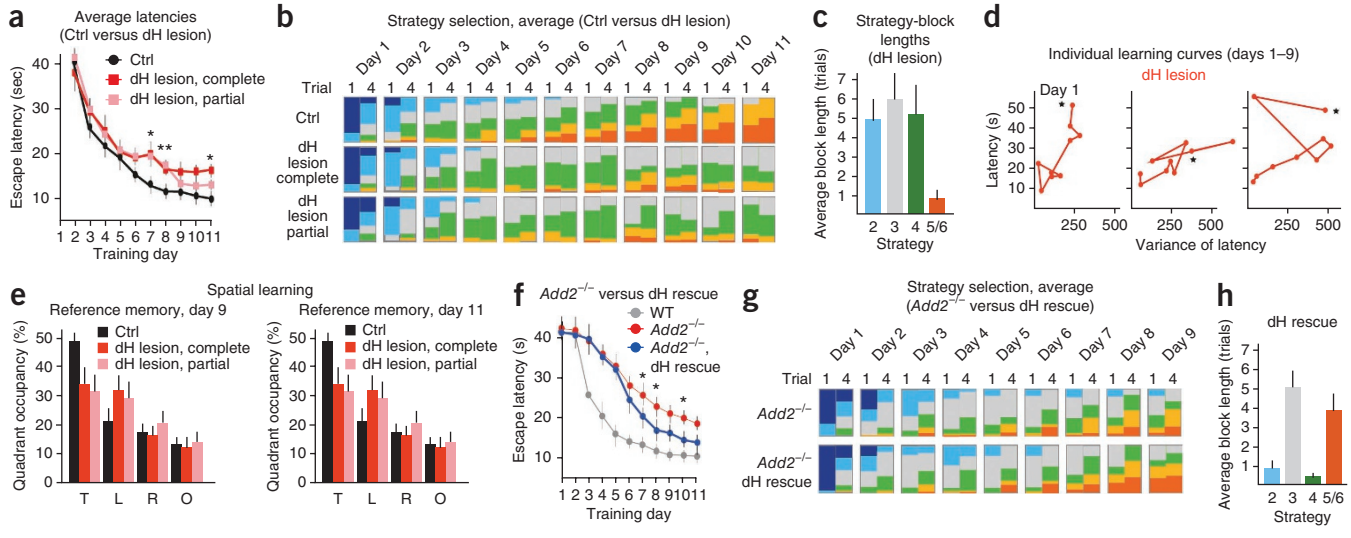

Figure 6 Function of dH in water maze learning. (**a**,**b**) Population-level analysis of latencies (**a**) and strategies (**b**) in mice with complete or partial excitotoxic lesions of dH versus controls. (**c**) Strategy-block lengths in dH-lesioned mice, as described in **Figure 1f**. (**d**) Variability of individual trials during maze learning in dH-lesioned mice (complete lesions). Latency versus latency variance is plotted for three individual mice. (**e**) Absence of fine-scale spatial learning (reference memory) in dH-lesioned mice (complete and partial lesions). Analysis in **a**–**h** as described in **Figure 4a**–**h**. $n = 8$ mice each (**a**–**e**). (**f**–**h**) Learning with FFI growth restricted to dH. There is specific rescue of late learning phase in *Add2*$^{-/-}$ mice upon reintroduction of β-adducin into granule cells of dH. Population and individual mouse analysis as described in **a**–**c**. $n = 12$ mice; Ctrl, control; WT, wild type. Error bars, s.e.m.; $^{*}P < 0.05$, $^{**}P < 0.01$.

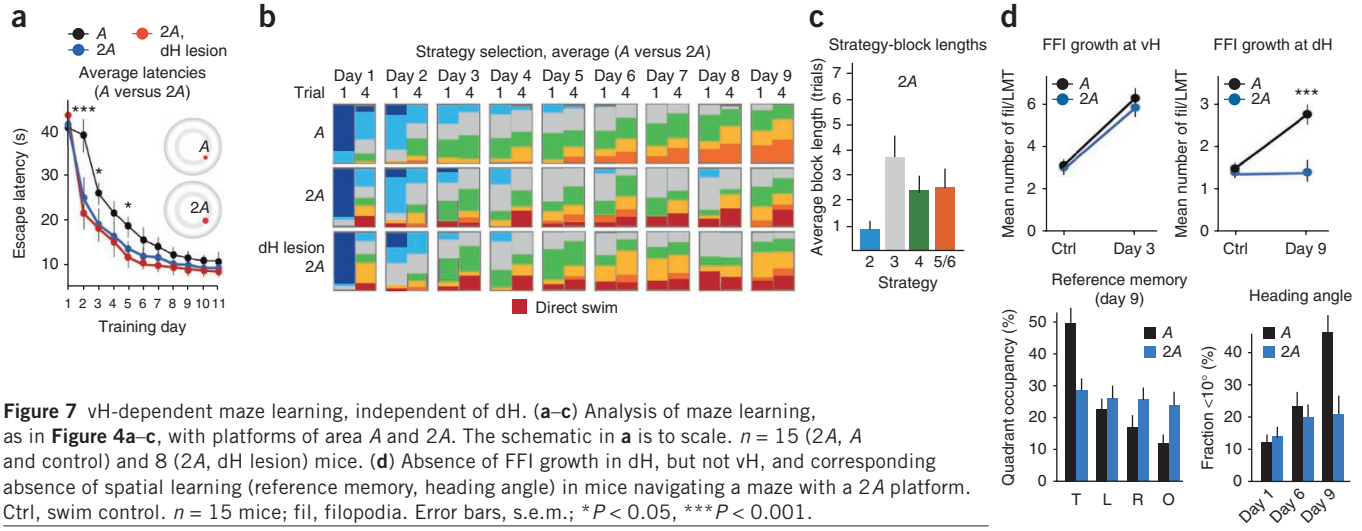

Figure 7 vH-dependent maze learning, independent of dH. (**a**–**c**) Analysis of maze learning, as in **Figure 4a**–**c**, with platforms of area *A* and 2*A*. The schematic in **a** is to scale. $n = 15$ (2*A*, *A* and control) and 8 (2*A*, dH lesion) mice. (**d**) Absence of FFI growth in dH, but not vH, and corresponding absence of spatial learning (reference memory, heading angle) in mice navigating a maze with a 2*A* platform. Ctrl, swim control. $n = 15$ mice; fil, filopodia. Error bars, s.e.m.; $^{*}P < 0.05$, $^{***}P < 0.001$.

strategy 4 = 6.12 ± 0.7, $P < 0.05$) and delayed deployment of spatial search strategies (**Fig. 5b**,**d**). Consistent with this delay in spatial search strategies, spatial reference memory in iH-lesioned mice was greatly impaired at day 9 but comparable to control reference memory values at day 11 (day 9 target quadrant occupancy = 47.8 ± 3% (vehicle), 34.2 ± 4% (iH lesion), $P < 0.05$; day 11 quadrant occupancy = 48.1 ± 5%, n.s. (iH lesion); **Fig. 5e**). Taken together, these results suggest that iH contributes during intermediate phases of water maze learning[33], when local search habits are deployed and spatial search habits have not yet emerged. Consistent with previous reports[16], the presence of an intact iH is not an absolute requirement for spatial learning.

Function of dH in water maze learning

Mice with bilateral excitotoxic dH lesions (**Supplementary Fig. 5**) were specifically impaired during the late phases (days 6–11) of maze learning (day 11 latency = 9.2 ± 2.3 s (control) and 16.5 ± 2.1 s (dH lesion), $P < 0.01$; **Fig. 6a**,**b**). dH-lesioned mice showed normal strategy deployments up to day 5 of training but failed to consistently deploy spatial search strategies during late phases of maze learning (average block length for strategy 5/6 = 0.9 ± 0.6 (dH lesion), $P < 0.001$; **Fig. 6b**,**c**). In addition, dH-lesioned mice did not show abnormally large variations in inter-trial latencies throughout maze learning (**Fig. 6d**; compare to **Fig. 4d**). Consistent with previous reports that dH is specifically required for spatial learning[14,16], mice with dH lesions did not establish a spatial reference memory (**Fig. 6e**). In control experiments, smaller, partial dH lesions with longitudinal extents comparable to those of the iH lesions (**Supplementary Fig. 5**; iH lesions: 800 ± 110 µm; complete dH lesions: 1,250 ± 120 µm; partial dH lesions: 600 ± 80 µm) produced late-phase learning latencies that were slightly better than those observed when complete dH lesions were present (**Fig. 6a**). Notably, however, the partial dH lesions also interfered with spatial searching (**Fig. 6b**) and suppressed establishment of reference memory (**Fig. 6e**), further supporting the notion that dH is specifically required for spatial learning whereas iH is not.

β-adducin rescue specifically in dH of *Add2*$^{-/-}$ mice markedly improved latencies at days 7–11 but did not influence latency values at days 3–5 of training (**Fig. 6f**). Consistent with a specific action of dH in spatial learning late during maze training, reintroduction of β-adducin in dH granule cells improved the progression of global spatial search strategies (**Fig. 6g**) and rescued the deployment of spatial search-strategy habits (average block length for strategies 5/6 = 0.84 ± 0.3 (*Add2*$^{-/-}$) and 3.95 ± 0.7 (dH rescue), $P < 0.001$; **Fig. 6h**), but it did not improve local strategy deployment (average block length for strategy 4 = 0.54 ± 0.1, n.s.; **Fig. 6g**,**h**) or the correlation between single-trial and mean latencies (**Supplementary Fig. 6**). These results suggest that dH is required specifically to establish a spatial map of the task during late phases of water maze learning and that learning processes involving vH or dH may be recruited independently of each other during a hippocampal spatial task.

vH-dependent maze learning, independent of dH

To investigate whether maze learning involving vH can occur in the absence of a requirement for dH, we modified the water maze task so that it would not require fine-scale spatial learning. We reasoned that if the area of the hidden platform were larger, mice would no longer need to systematically apply spatial search strategies to effectively locate it. Indeed, when the standard platform area (*A*) was doubled from 78.5 cm^2 (corresponding to 10 cm in diameter) to 157 cm^2 (14 cm diameter, in a pool of diameter 140 cm), mice learned the task more rapidly (day 2 latency = 38.9 ± 4.6 s (*A*) and 23.8 ± 2.1 s (2*A*), $P < 0.001$; **Fig. 7a**). Mice also showed directed search and direct swim on the fourth trial throughout the training process (that is, they took 'shortcuts'), but they did not show a consistent increase in the application of spatial search strategies during the second half of the training procedure (**Fig. 7b**,**c**). In what is probably a reflection of less challenging learning conditions and the successful application of 'shortcuts', the analysis of individual mice revealed a reduced deployment of habits (**Supplementary Fig. 1** and **Fig. 7c**). Notably, although vH FFI growth was indistinguishable between the two platform areas (day 3 filopodia/LMT = 5.94 ± 0.7 (*A*) and 6.1 ± 0.8 (2*A*), n.s.), mice developed no reference memory of the platform quadrant (day 9 average target quadrant occupancy = 49.8 ± 4% (*A*) and 28.3 ± 2% (2*A*), $P < 0.01$) and did not learn to head directly for the platform between day 7 and day 9 of training. Further, mice did not show an increase in dH filopodia/LMT under 2*A* platform conditions (filopodia/LMT =1.7 ± 0.1 (swim control), 2.88 ± 0.2 (*A*, day 9) and 1.74 ± 0.1 (2*A*, day 9), n.s.; **Fig. 7d**). iH filopodia/LMT also did not increase under 2*A* platform conditions (at day 9; data not shown). Consistent with the notion that dH is not required for mice to learn to navigate a maze with a 2*A* platform, learning curves and strategy progressions were indistinguishable between mice with complete dH lesions and controls under 2*A* conditions (day 2 latency = 22.5 ± 2.1 (control) and 20.8 ± 1.8 (dH lesions), n.s.; **Fig. 7a**,**b**).

DISCUSSION

Our detailed behavioral analysis of how individual mice learn to navigate a water maze—a biologically relevant task—combined with the analysis and local manipulation of its specific anatomical counterparts in the hippocampus, provides insights into the mechanisms of complex trial-and-error learning. We provide evidence that maze navigation involves a stereotyped sequence of subtasks that involve learning at distinct hippocampal subdivisions. The connectivity and functions of hippocampal subdivisions may thus influence how the individuals of a species address declarative trial-and-error tasks involving the hippocampus. Our results further reveal that vH is crucial early in goal-oriented learning and searching, and they thus assign a key function to vH (anterior hippocampus in humans) in complex behavioral learning.

Our longitudinal analysis of water maze learning has revealed the presence of a structured learning process throughout the training procedure, as indicated by the sequential roles of vH, iH and dH during maze learning and the sequential deployment of increasingly sophisticated spatial search habits (**Supplementary Fig. 8**). The mechanisms linking successful subtask learning to FFI growth at hippocampal subdivisions remain to be determined and may differ among individual networks. For example, vH switches appear to occur abruptly, whereas incremental FFI growth at iH and dH during maze learning may be coupled to gradual error-function mechanisms[3,30]. In a possibly related issue, the mechanisms underlying strategy selection and the establishment of search habits[3,5] also remain to be determined. Because basal ganglia systems have prominent roles in the adjustment of learning and habits to performance through dopamine-mediated reward systems[3,5,30], it is tempting to speculate that the processes of strategy selection discovered in this study may involve cost-reward computations at striatal circuits. This possibility seems particularly plausible for learning involving vH, which has extensive connectivity with striatal circuitry[15,21].

Our study assigns a key function to vH in the early stages of complex trial-and-error learning. We provide evidence that FFI growth at vH reflects previous behavioral learning of consistent task-specific goal-context relationships and supports deployment of local search habits during further learning and that an intact vH is crucial in supporting performance consistency throughout maze learning. These results tie in well with previous reports that 'simplified learning', which consists of pre-training rats with a visible platform (a task involving learning in vH), accelerates subsequent maze learning and reduces its requirement for NMDA-mediated plasticity[34,35]. Previous studies have not assigned functions to vH in hippocampus-dependent spatial learning. That may be owing to a predominant focus on the endpoint of complex hippocampus-dependent learning, which usually involves cognitive and highly spatial aspects depending on dH, and to the fact that most studies have not focused on how learning is achieved longitudinally by individual animals[36]. However, previous studies have provided evidence that vH lesions impair aversive learning and reduce anxiety[15,37], and these findings are consistent with the notion that vH has a crucial function in relating reinforcers to context in learning. The strong direct connectivity of vH with body state and emotional and reward systems[15] might underlie its early function in goal-oriented learning and searching. Although it is possible that all hippocampal subdivisions participate in the learning process from its onset, vH might be more directly tuned to the detection and consolidation of consistent associations between goal and local task-specific features. According to this hypothesis, subsequent support of increasingly spatial and cognitive networks involving first iH and then dH might involve indirect connectivity of iH and dH with ventral reward-linked networks—for example, via thalamic nuclei and/or peri-postrhinal cortices[15]. Whether and how the specific connectivities of hippocampal subdivisions underlie their hierarchical recruitment during goal-oriented, trial-and-error learning remain to be determined, however. Our results provide evidence that vH acts in maze learning up to day 6, and they suggest a partially overlapping and later function for iH. The function of iH is poorly understood, but it can mediate rapid place learning[33] and has been suggested to integrate ventral and dorsal functions in hippocampus-dependent behavioral learning[15,33]. One possibility consistent with our findings is that FFI growth at vH on day 3 is important to support place learning mediated by iH between days 3 and 6 (**Supplementary Fig. 8**).

The assignment to vH of a crucial function in early goal-oriented learning has implications for future research. Thus, efficient goal-oriented learning and searching and rapid mastering of intermediate goals are likely to be key determinants of success in realistic biological settings. Furthermore, the linkage of emotional processes to declarative learning through vH may affect behavioral learning in emotionally complex settings, including social interactions. Accordingly, it will be of interest to determine how vH influences the learning of emotionally complex tasks under healthy and pathologic conditions.

METHODS

Methods and any associated references are available in the online version of the paper.

Note: Supplementary information is available in the online version of the paper.

ACKNOWLEDGMENTS

We thank B. Sacchetti (University of Torino), C. Sandi (École Polytechnique Fédérale de Lausanne) and S. Arber (Friedrich Miescher Institut) for comments on the manuscript. The Friedrich Miescher Institut is part of the Novartis Research Foundation.

AUTHOR CONTRIBUTIONS

S.R. devised and carried out the analysis of hippocampal behavior, connectivity, vH lesions and β-adducin rescue; D.S. carried out the analysis of FFI growth and c-Fos immunoreactivity; F.D. devised and carried out behavioral and lesion studies relating vH, iH and dH FFI growth to subdivision function in learning. P.C. helped devise the experiments and wrote the manuscript. All authors discussed the results and commented the manuscript.

COMPETING FINANCIAL INTERESTS

The authors declare no competing financial interests.

Published online at http://www.nature.com/doifinder/10.1038/nn.3224.
Reprints and permissions information is available online at http://www.nature.com/reprints/index.html.

1. Sutton, R.S. & Barto, A.G. *Reinforcement Learning: An Introduction* (MIT Press, 1998).
2. Dayan, P. & Balleine, B.W. Reward, motivation and reinforcement learning. *Neuron* **36**, 285–298 (2002).
3. Graybiel, A.M. Habits, rituals, and the evaluative brain. *Annu. Rev. Neurosci.* **31**, 359–387 (2008).
4. Barnes, T.D., Kubota, Y., Hu, D., Jin, D.Z. & Graybiel, A.M. Activity of striatal neurons reflects dynamic encoding and recoding of procedural memories. *Nature* **437**, 1158–1161 (2005).
5. Desrochers, T.M., Jin, D.Z., Goodman, N.D. & Graybiel, A.M. Optimal habits can develop spontaneously through sensitivity to local cost. *Proc. Natl. Acad. Sci. USA* **107**, 20512–20517 (2010).
6. Thorn, C.A., Atallah, H., Howe, M. & Graybiel, A.M. Differential dynamics of activity changes in dorsolateral and dorsomedial striatal loops during learning. *Neuron* **66**, 781–795 (2010).
7. Amemori, K., Gibb, L.G. & Graybiel, A.M. Shifting responsibility: the importance of striatal modularity to reinforcement learning in uncertain environments. *Front. Hum. Neurosci.* **5**, 47 (2011).
8. Botvinick, M.M., Niv, Y. & Barto, A.C. Hierarchically organized behavior and its neural foundations: a reinforcement-learning perspective. *Cognition* **113**, 262–280 (2009).
9. O'Keefe, J. & Nadel, L. *The Hippocampus as a Cognitive Map* (Oxford Univ. Press, 1978).
10. Moser, E.I., Kropff, E. & Moser, M.B. Place cells, grid cells, and the brain's spatial representation system. *Annu. Rev. Neurosci.* **31**, 69–89 (2008).

11. Bird, C.M. & Burgess, N. The hippocampus and memory: insights from spatial processing. *Nat. Rev. Neurosci.* **9**, 182–194 (2008).
12. Morris, R.G.M., Garrud, P., Rawlins, J.N.P. & O'Keefe, J. Place navigation impaired in rats with hippocampal lesions. *Nature* **297**, 681–683 (1982).
13. Moser, M.B. & Moser, E.I. Functional differentiation in the hippocampus. *Hippocampus* **8**, 608–619 (1998).
14. Dong, H.W., Swanson, L.W., Chen, L., Fanselow, M.S. & Toga, A.W. Genomic-anatomic evidence for distinct functional domains in hippocampal field CA1. *Proc. Natl. Acad. Sci. USA* **106**, 11794–11799 (2009).
15. Fanselow, M.S. & Dong, H.-W. Are the dorsal and ventral hippocampus functionally distinct structures? *Neuron* **65**, 7–19 (2010).
16. Moser, M.B., Moser, E.I., Forrest, E., Andersen, P. & Morris, R.G.M. Spatial learning with a minislab in the dorsal hippocampus. *Proc. Natl. Acad. Sci. USA* **92**, 9697–9701 (1995).
17. Thompson, C.L. *et al.* Genomic anatomy of the hippocampus. *Neuron* **60**, 1010–1021 (2008).
18. Viard, A., Doeller, C.F., Hartley, T., Bird, C.M. & Burgess, N. Anterior hippocampus and goal-directed spatial decision making. *J. Neurosci.* **31**, 4613–4621 (2011).
19. Royer, S., Sirota, A., Patel, J. & Buzsaki, G. Distinct representations and theta dynamics in dorsal and ventral hippocampus. *J. Neurosci.* **30**, 1777–1787 (2010).
20. Young, J.J. & Shapiro, M.L. Dynamic coding of goal-directed paths by orbital prefrontal cortex. *J. Neurosci.* **31**, 5989–6000 (2011).
21. Pennartz, C.M., Ito, R., Verschure, P.F., Battaglia, F.P. & Robbins, T.W. The hippocampal-striatal axis in learning, prediction and goal-directed behavior. *Trends Neurosci.* **34**, 548–559 (2011).
22. Ruediger, S. *et al.* Learning-related feedforward inhibitory connectivity growth required for memory precision. *Nature* **473**, 514–518 (2011).
23. Bednarek, E. & Caroni, P. β-adducin is required for stable assembly of new synapses and improved memory upon environmental enrichment. *Neuron* **69**, 1132–1146 (2011).
24. Morris, R. Development of a water-maze procedure for studying spatial learning in the rat. *J. Neurosci. Methods* **11**, 47–60 (1984).
25. Wolfer, D.P. & Lipp, H.P. Dissecting the behaviour of transgenic mice: is it the mutation, the genetic background, or the environment? *Exp. Physiol.* **85**, 627–634 (2000).
26. Janus, C. Search strategies used by *APP* transgenic mice during navigation in the Morris water maze. *Learn. Mem.* **11**, 337–346 (2004).
27. Garthe, A., Behr, J. & Kempermann, G. Adult-generated hippocampal neurons allow the flexible use of spatially precise learning strategies. *PLoS ONE* **4**, e5464 (2009).
28. Luo, A.H., Tahsili-Fahadan, P., Wise, R.A., Lupica, C.R. & Aston-Jones, G. Linking context with reward: a functional circuit from hippocampal CA3 to ventral tegmental area. *Science* **333**, 353–357 (2011).
29. Wiltgen, B.J. *et al.* The hippocampus plays a selective role in the retrieval of detailed contextual memories. *Curr. Biol.* **20**, 1336–1344 (2010).
30. Schultz, W., Dayan, P. & Montague, P.R. A neural substrate of prediction and reward. *Science* **275**, 1593–1599 (1997).
31. Bethus, I., Tse, D. & Morris, R.G.M. Dopamine and memory: modulation of the persistence of memory for novel hippocampal NMDA receptor-dependent paired associates. *J. Neurosci.* **30**, 1610–1618 (2010).
32. Rabenstein, R.L. *et al.* Impaired synaptic plasticity and learning in mice lacking β-adducin, an actin-regulating protein. *J. Neurosci.* **25**, 2138–2145 (2005).
33. Bast, T., Wilson, I.A., Witter, M.P. & Morris, R.G.M. From rapid place learning to behavioral performance: a key role for intermediate hippocampus. *PLoS Biol.* **7**, e1000089 (2009).
34. Bannerman, D.M., Good, M.A., Butcher, S.P., Ramsay, M. & Morris, R.G.M. Distinct components of spatial learning revealed by prior training and NMDA receptor blockade. *Nature* **378**, 182–186 (1995).
35. Hoh, T., Beiko, J., Boon, S., Weiss, S. & Cain, D.P. Complex behavioral strategy and reversal learning in the water maze without NMDA receptor-dependent long-term potentiation. *J. Neurosci.* **19**, RC2 (1999).
36. Gallistel, C.R., Fairhust, S. & Balsam, P. The learning curve: implications of a quantitative analysis. *Proc. Natl. Acad. Sci. USA* **101**, 13124–13131 (2004).
37. Kjelstrup, K.G. *et al.* Reduced fear expression after lesions of the ventral hippocampus. *Proc. Natl. Acad. Sci. USA* **99**, 10825–10830 (2002).

ONLINE METHODS

Reagents and anatomical procedures. *Add2*$^{-/-}$ mice[32] were from Jackson Laboratories, Bar Harbor, Maine; the reporter line *Thy1-mGFP(Lsi1)* was as described[38]. The GFP-β-adducin construct was cloned into a lentivirus vector, and dentate gyrus infections were done as described[9]. We analyzed structural traces of learning at GFP-positive LMTs of ventral and dorsal hippocampus (CA3b) using the 'sparse' transgenic reporter line *Thy1-mGFP(Lsi1)*[22]. In parallel, the main findings were confirmed in mice in which we labeled mossy fibers randomly using a lentivirus expressing membrane-targeted GFP (mGFP)[22]. On the basis of boundaries identified by previous gene-expression studies[14,17], we defined subdivisions along the dorsoventral axis of the hippocampus as follows: dorsal, within 20–30% of total length; intermediate, within 45–55%; ventral, within 70–80%.

Behavioral procedures and their analysis. Mice were kept in temperature-controlled rooms on a constant 12-h light-dark cycle, and all experiments were conducted at approximately the same time of the light cycle. Before the behavioral experiment, mice were housed individually for 3–4 d and provided with food and water *ad libitum* unless otherwise stated. All animal procedures were approved and performed in accordance with the Veterinary Department of the Canton Basel-Stadt.

All behavioral experiments were carried out with male mice that were 55–65 d old at the onset of the experiment and were performed according to standard procedures[22,23].

The Morris water maze consisted of a circular (diameter: 140 cm) pool filled with opaque water at 24 °C. The circular escape platform (10 cm in diameter) was positioned at a fixed position 0.5 cm above (visible) or 0.5 cm below the water (hidden). Training involved four 60-s trials separated by 5-min intervals every day. For each trial, mice were placed at random starting locations in the pool facing the pool wall. At the end of each trial, mice were allowed to sit on the platform for 15 s; when trials were unsuccessful, mice were manually guided to the platform. Latencies and reference memories were determined as described. Heading angles were determined using the starting position of the mouse, a line connecting that position to the platform and a second line connecting the start position to the position of the mouse after swimming 18 cm. We selected this distance to exclude variations due to initial rotations away from the pool wall.

We collected and analyzed data from training sessions and probe trials using Viewer2 Software (Biobserve, Bonn, Germany). The software Viewer III (Biobserve) was used to sample animal positions during Morris water maze trials. Search strategies were as defined in previous studies[25,27]. For quantitative identification of search strategies, we developed an algorithm in collaboration with Biobserve. We corrected all swimming trajectories to compensate for errors owing to incorrect object detection during the first 1.5 ± 1 s of tracking (for example, water movement caused by immersion of the mouse close to the border or experimenter's hand). We further corrected tracking to start subsequent to a 90° turn (away from the wall) around the center of a 5-cm radius defining the immersion point (center of gravity of the mouse body). Chaining annulus and direct-swimming corridor were adjusted accordingly, and prevailing strategies were then assigned automatically by the software's algorithm. Search strategies were defined as follows[27]: thigmotaxis: >35% of swim time (60 s) within closer wall zone (5 cm from pool wall) and >65% of time within wider wall zone (10 cm from pool wall); random search: >70% surface coverage; scanning: <70% surface coverage and >15% surface coverage <0.7 s.d. distance to the pool center; chaining: >65% of time within annulus zone; directed search: >80% of time in goal corridor (rectangular goal corridor 20 cm wide, centered along direct connection between start and platform positions); focal search: <0.35 s.e.m. body angle, <0.25 s.d. mean distance to present goal; direct swim: 100% in goal corridor. When we used these definitions and the algorithm in combination with the adjustments described above, only <3% of the trials could not be assigned univocally to one strategy. Strategy blocks were defined as a sequence of at least three trials with the same strategy (or two trials for blocks of strategies 5 and 6). For block lengths, one-trial interruptions were tolerated but not counted (for example, a 2225223422 sequence was scored as a block length of 5 for strategy 2). Total block lengths were the sum of all blocks for one strategy and one mouse. For strategy/latency deviation values, mean latencies within days 1–2, days 3–6 and days 7–9 for a particular condition or genotype were subtracted from corresponding single-trial latencies when the strategies of those trials deviated from those of a sequence of at least two trials involving the same strategy by at least two strategy levels (for example, latency of the fourth trial in the sequence 222422). Statistical analyses were performed using Student's *t*-tests and one-way ANOVA; $P < 0.05$ in *post hoc* comparisons. Results are presented as mean ± s.e.m.

For fear-conditioning experiments, the conditioning chamber was cleaned with 2% acetic acid before and after each session. Once placed inside the training chamber, mice were allowed to explore the apparatus for 2.5 min, and then they received a series of five footshocks (1 s and 0.8 mA each, inter-trial interval of 30 s). Control mice were subjected to the same procedure without receiving footshocks. We assessed contextual fear memory by returning mice to the training chamber 24 h after fear conditioning during a test period of 2.5 min. Freezing was defined as the complete absence of somatic mobility other than respiratory movements. Fear conditioning in the dark involved the same procedure but with all lights switched off. Recall 24 h after conditioning was in the following training context: in the presence of odor A (2% acetic acid) or B (0.25% benzaldehyde) and on a shock floor or plastic floor.

For novel-object recognition experiments, mice were first habituated to the testing arena for 10 min. On the next day, each animal was allowed to explore two identical objects placed in the arena for 10 min. Twenty-four hours later, mice explored the same arena for 5 min, with one of the familiar objects replaced by a novel object. Recognition memory was expressed by the discrimination index (D), which was defined as $D = (T(\text{novel}) - T(\text{familiar})) / (T(\text{novel}) + T(\text{familiar}))$.

For the reinforced-learning version of the object recognition task and its controls, we fed all mice sufficiently only after each training session to maintain their body weight at 85% of their initial weight. Wheat flakes (three to five flakes; 100–120 mg in total) were placed as a reward on top of the familiar object (a cube of ~4 cm in height with an inserted cylinder of an additional 3 cm in height; reward flakes were placed on top of the cube and the cylinder). To habituate mice to the reward, we placed two to three wheat flakes in the home cages after each habituation and training session. For all object recognition task protocols, we cleaned the testing arena with 70% ethanol after each mouse on each day.

Drug delivery and stereotactic surgery *in vivo*. SCH23390 (Tocris Bioscience) was dissolved in saline 0.9% and injected i.p. at a doses of 0.05 mg/kg 20 min before water maze training at day 1 (habituation) and throughout the training. Coordinates for lentiviral injections into mouse dentate gyrus were (in mm from Bregma): 1.70 posterior, 1.10 lateral, 1.70 down (dorsal hippocampus); 3.16 posterior, –2.5 lateral, 2.10 down (ventral hippocampus). The lentivirus for β-adducin rescue was as described[9]. *Add2*$^{-/-}$ mice were trained 5 weeks after injection of eGFP–β-adducin lentivirus. For hippocampal subdivision lesions, ibotenic acid (Ascent Scientific) was dissolved in PBS to a final concentration of 10 mg/ml, and injections of 50 nl were made at two or three sites. Injections coordinates were (in mm from Bregma): 3.08 posterior; 2.7 lateral; 3.2, 3.4 and 3.6 down (vH lesion); 2.3 posterior; 2.3 lateral: 1.3, 1.5 and 1.7 down (iH lesion); 1.58 posterior; 1.25 lateral; 1.3 and 1.6 down (dH lesion, complete). Upon injection, mice were given 7 d recovery before training.

Immunocytochemistry and histology. Antibodies were as follows: rabbit antibody to GFP (Molecular Probes, Eugene, OR, USA), 1:1,000; rabbit antibody to c-Fos (Santa Cruz; sc-253), 1:10,000; mouse antibody to NeuN (Chemicon; MAB377), 1:200. Secondary antibodies were Alexa Fluor 568 (Molecular Probes; A10037 or 488 (Molecular Probes; A11008); 1:500.

Morris water maze, c-Fos expression. Mice performed a single probe trial 24 h after the final training session and were returned to their home cage for 90 min before perfusion (transcardially with 4% PFA in PBS, pH 7.4). Brains were kept in fixation solution overnight at 4 °C. Hippocampi were dissected, embedded in 3% agarose gel and sliced transversally on a tissue chopper (McIlwain) to yield lamellar hippocampal sections of 100-µm thickness. c-Fos immunocytochemistry was performed and analyzed as described[21].

Imaging and image analysis. For high-resolution imaging of LMTs in fixed tissue, we imaged lamellar sections on an upright spinning-disk microscope using an alpha Plan-Apochromat ×100/1.45 oil-immersion objective (Zeiss) and Metamorph 7.7.2 acquisition software (Molecular Devices, Sunnyvale, CA, USA). Voxel size was 0.106 µm × 0.106 µm × 0.2 µm. For c-Fos analysis, we processed all samples belonging to the same experimental set in parallel and acquired them with the same settings on an LSM700 confocal microscope (Zeiss) using an EC

doi:10.1038/nn.3224

Plan-Neofluar ×40/1.3 oil-immersion objective (Zeiss). We used transverse hippocampal sections at different dorsoventral levels (dorsal, intermediate and ventral hippocampus) for the analysis of LMT morphology and filopodial contents in CA3b. We analyzed 80–100 LMTs per animal and region; this involved three to four confocal stacks per section along CA3b and an average of three to four sections. We analyzed all objects that were completely included in the three-dimensional stack blind to experimental conditions. We analyzed high-resolution three-dimensional confocal stacks using Imaris 7.0.0 (Bitplane AG) software.

38. De Paola, V., Arber, S. & Caroni, P. AMPA receptors regulate dynamic equilibrium of presynaptic terminals in mature hippocampal networks. *Nat. Neurosci.* **6**, 491–500 (2003).